SUBMISSION TO GEOMECHANICS FOR ENERGY AND THE ENVIRONMENT
SPECIAL ISSUE: "VSI: Low Carbon Geotechnics"

DATE:
Written 3rd August 2020
Revised 7th April 2021

TITLE:
Hydraulic behaviour of fungal treated sand

AUTHORS:
Emmanuel Salifu (BEng, MSc, PhD).[1,2]
Gráinne El Mountassir (MEng, PhD)[3]
James Minto (MEng, PhD)[4]
Alessandro Tarantino (MEng, PhD)[5]

POSITION AND AFFILIATION:
[1] Research Associate - Department of Civil & Environmental Engineering, University of Strathclyde, Glasgow, UK
[2] Researcher - Università di Napoli, Dipartimento di Ingegneria Civile, Edile e Ambientale, Federico II, Italy
[3] Senior Lecturer - Department of Civil & Environmental Engineering, University of Strathclyde, Glasgow, UK
[4] Chancellor's Fellow (Lecturer) - Department of Civil & Environmental Engineering, University of Strathclyde, Glasgow, UK
[5] Professor - Department of Civil & Environmental Engineering, University of Strathclyde, Glasgow, UK

CORRESPONDING AUTHOR:
Dr Gráinne El Mountassir
Senior Lecturer
Department of Civil & Environmental Engineering
University of Strathclyde
James Weir Building
75 Montrose Street
Glasgow
G1 1XJ
Telephone: +44 (0)141 548 3275 (Department reception)
E-mail:grainne.elmountassir@strath.ac.uk

NUMBER OF WORDS, FIGURES AND TABLES
8162 words, 12 Figures, 02 Tables

47 **HYDRAULIC BEHAVIOUR OF FUNGAL TREATED SAND**

48 **Salifu, E., El Mountassir, G., Minto, J., and Tarantino, A.**

49 **ABSTRACT**

50 Engineered growth of the saprotrophic fungus *Pleurotus ostreatus* has recently been
51 observed to induce water repellency in sands. As such, there is potential for the
52 deployment of fungi to reduce water infiltration in granular soils. In this study, we
53 investigate the influence of the growth of *P. ostreatus* on the hydraulic behaviour of a
54 sand amended with organic matter (lignocellulose) over a 12-week period. This
55 includes investigation of the water retention and quasi-saturated hydraulic
56 conductivity properties and the response to ponded infiltration. Furthermore, we
57 investigate alterations to soil microstructure due to fungal growth using X-ray micro-
58 computed tomography. Fungal treatment resulted in a shift in the wetting curves to
59 lower suctions and drying curves to higher suctions, lower quasi-saturated hydraulic
60 conductivity, and lower ponded infiltration rates. These alterations to the hydraulic
61 behaviour are attributed to combined biochemical and biophysical effects of fungal
62 growth leading to clogging of some soil pores by fungal hyphal biomass. These results
63 illustrate the potential for the deployment of fungal treatment as a low-cost technology
64 suitable for application at catchment-scale which could be used to enhance the stability
65 of shallow slopes, cut slopes and retaining walls by maintaining higher soil suction
66 and shear strength after rainfall events.

67 **Keywords:** ground improvement, fungal mycelium, infiltration, soil water retention,
68 quasi-saturated hydraulic conductivity, fungal mycelium

1 Introduction

Water infiltration into soils results in an increase in pore-water pressure and an associated reduction in soil shear strength. In coarse-grained soils, this mechanism is responsible for triggering failures after periods of heavy rain, including (i) shallow landslides in natural slopes (e.g. Olivares and Picarelli, 2004; Springman, Jommi and Teysseire, 2004; Balzano, Tarantino and Ridley, 2019), (ii) failures in engineered slopes of industrial waste (Fourie, Rowe and Blight, 1999), (iii) instability of vertical cuts (Stanier and Tarantino, 2013) and (iv) failure of retaining walls (Scotto di Santolo, Evangelista and Evangelista, 2017).

Remedial measures over extensive areas on natural slopes typically include soil nailing, geosynthetic reinforcement, ground stabilisation and drainage control. Traditional techniques use materials (e.g. cement, iron and steel) with a high embedded carbon and are most suited to targeting localised instabilities. Vegetation on the other hand is increasingly being considered as an engineering option due to its low-cost, ability to fix carbon and be deployed at a catchment-scale (Greenwood, Norris and Wint, 2004; Stokes *et al.*, 2013). Vegetation can provide mechanical reinforcement (e.g. Waldron, 1977; Veylon *et al.*, 2015) and induce beneficial hydrological/hydraulic effects. These effects include the interception of rainfall, enhanced soil water extraction via plant transpiration, fine root systems (<1mm) acting to clog pores and reduce soil hydraulic conductivity, all contributing towards maintaining higher soil suction, and higher shear strength (Pollen-Bankhead and Simon, 2010; Ng *et al.*, 2013; Stokes *et al.*, 2013; Leung et al., 2015; Boldrin, Leung and Bengough, 2020; Lu et al., 2020). On the other hand, studies have reported that thick roots can promote the formation of macropores, enhancing near-surface soil hydraulic conductivity and infiltration (e.g. Angers & Caron, 1998; Lu et al., 2020). While this may act to divert subsurface flow laterally acting as a drainage layer and reduce infiltration of rainwater to deeper soil layers (Balzano, Tarantino and Ridley, 2019) in other soil-plant systems increased soil hydraulic conductivity, enhanced infiltration and preferential flow via thick roots can have a negative influence,

98 resulting in reduced soil suction at depth and contribute to slope instability (Ghestem,
99 Sidle and Stokes, 2011; Dias, 2019).

100 Recently synthetic water repellent soils created via organosilanes have been proposed
101 for creating semi-permeable barriers on natural slopes to reduce infiltration; however,
102 such treatment can lead to an in increase in soil erosion (depending on soil type)
103 (Lourenço, Wang and Kamai, 2015; Zheng *et al.*, 2017, 2019). Salifu and El
104 Mountassir, (2020) proposed that water repellency could be engineered via fungal
105 growth in sand using the saprotrophic fungus *Pleurotus ostreatus* (*P. ostreatus*). They
106 demonstrated that extreme levels of water repellency (characterised by macroscopic
107 contact angles > 110^{o} as measured via modified sessile drop method) could be
108 achieved in sands treated with *P. ostreatus* after 1 week of growth, and severe water
109 repellency (contact angles >105^{o}) was sustained for the duration of the 12-week
110 growth period in depleting nutrient and moisture conditions.

111 Fungi are ubiquitous and diverse organisms. Based on their mode of nutrition, soil
112 fungi can be broadly classified into three main groups (i) saprotrophic fungi which
113 decompose dead organic matter, (ii) parasitic fungi that colonise hosts and (iii)
114 symbionts that exist in a mutually beneficial symbiotic relationship with plants, which
115 include mycorrhizal species. Multi-cellular filamentous fungi grow as hyphae, which
116 are elongated tubular structures, which enable the fungus to access nutrient sources.
117 Hyphae typically have diameters in the range of 1-30μm and lengths from several
118 microns to several metres (Islam *et al.*, 2018). As hyphal growth continues, hyphae
119 can branch into multiple hyphae and can anastomose; the network of hyphae is
120 collectively known as the mycelium. Figure 1a shows typical growth of *P. ostreatus*
121 in sand (with 1% organic matter) growing radially from a central inoculation source,
122 with the mycelium visible in white. Figure 1b demonstrates the water-repellent nature
123 of the sand surface due to mycelium growth.

124 Mycorrhizal and saprotrophic fungi are known to contribute to soil aggregate stability
125 in nature via physical enmeshment of soil particles with hyphae and the exudation of
126 biochemicals which promote adhesion (Rillig and Mummey, 2006). Furthermore, soils

127 with fungal activity have been shown to exhibit enhanced resistance to wind and
128 water-induced erosion (Vogelsang *et al.*, 2004; Tisdall *et al.*, 2012; Mardhiah *et al.*,
129 2016). Unlike mycorrhizal species, which are dependent on the availability of suitable
130 symbiotic plants (and their required growing conditions), saprotrophic fungi could be
131 deployed independently as a remedial measure to reduce infiltration and maintain soil
132 suction in slopes. Thus, they could have additional application on natural and
133 engineered slopes for example on non-vegetated bare soil surfaces, (i.e. immediately
134 after landslides) without the need for plant colonisation, provided that adequate
135 nutrients are available or can be provided to sustain the organisms.

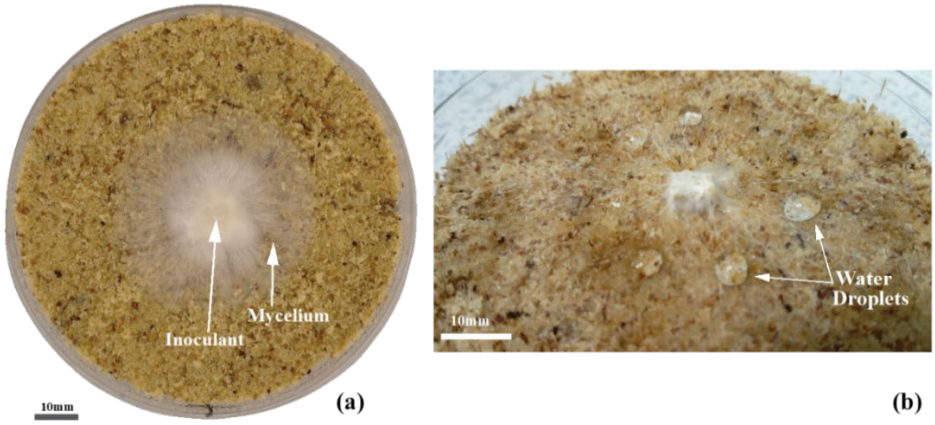

136

137 *Figure 1. Mycelium of Pleurotus ostreatus growing radially from a spores-colonised substrate on sand*
138 *amended with 1% lignocellulose, w_i=11%. (a) Mycelial extent 4 days after inoculation (b) Water*
139 *droplets on the surface of the sample after 4 weeks growth indicating mycelium induced water*
140 *repellency.*

141 The overall aim of this paper is to experimentally investigate the hydraulic behaviour
142 of sand treated with the saprotrophic fungus *P. ostreatus,* in order to assess its potential
143 suitability as a technology for reducing infiltration. Specifically, the objectives are to
144 compare (i) the soil water retention behaviour, (ii) the quasi-saturated hydraulic
145 conductivity and (iii) the response to ponded infiltration of a sand in which fungal
146 growth took place over a 12-week period, with that of corresponding untreated control
147 specimens. Evolution of the soil microstructure due to fungal growth is also
148 investigated.

2 Materials and sample preparation

2.1 Soil

A poorly-graded silica sand with Coefficient of Uniformity, C_u = 3.6; Coefficient of Curvature, C_c = 1.1) was used in this study, (classification based on BS EN ISO 14688-2:2018). The particle size distribution of the sand was determined via dry sieving as shown in Figure 2. The sand was mixed with lignocellulose at 5.5% of the total mass of solids to form the soil composition. Lignocel® (HB 500 – 1000) is a commercially packaged natural softwood fibre processed and marketed by J. RETTENMAIER & SÖHNE GmbH. It is used in this study to serve as the organic substrate (i.e. nutrient source) for fungal growth. Lignocel has a total organic carbon content of 524 ± 7 g/kg and total nitrogen content of 1.5 ± 0.01g/kg, giving a carbon/nitrogen ratio of ~350. The particle size distribution of the lignocellulose, determined via dry sieving is also presented in Figure 2.

2.2 Fungal suspension

Pleurotus ostreatus (strain: M 2191) supplied by GroCycle UK in the form of active fungal spawn (fungal mycelium grown on a wheat substrate) was used in this study. It was stored at 4°C and used within 10 days after delivery.

Inoculation of the soil was carried out using a spore/hyphal suspension of *P. ostreatus,* hereafter referred to as the fungal suspension. The fungal suspension was prepared by placing 50g of fungal spawn in a 500 mL conical flask containing deionised water (DI) and subjecting it to vigorous shaking, manually, for 30mins in order to release spores and hyphae into the water. The liquid was then filtered through a 2 mm sieve to remove any large solid mycelium fragments and spawn grains from the final fungal suspension. The suspension was freshly prepared each time and used to inoculate the soil specimens within 1-2 hours after preparation.

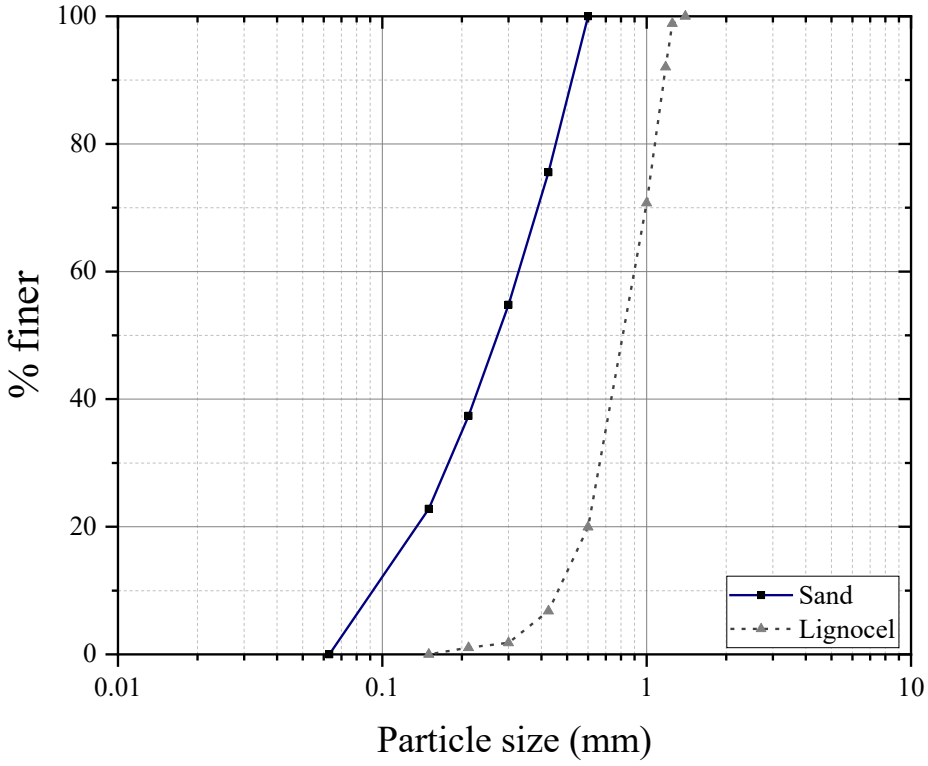

Figure 2. Particle size distributions of the sand and lignocellulose

2.3 Preparation of samples for incubation

The sand was thoroughly mixed with lignocellulose in the proportions shown in Table 1. The sand-lignocellulose mixture was autoclaved at 121°C for 20mins to ensure the material was initially sterile. Under aseptic conditions, 283 cm^3 of fungal suspension was added to the soil material and manually mixed in a bowl. For untreated specimens the same volume of DI water was used in place of the fungal suspension.

Table 1: Composition and characteristics of samples

Sample	Sample composition & characteristics					
	Mass of sand (g)	Mass of lignocel (g)	Liquid content* (w)	Initial Dry Density (kg/m^3)	Initial Porosity$^{\downarrow}$ (n)	Degree of saturation (S_r)
Treated	2403	141	Fungal suspension: 0.11	1080	0.58	0.21
Untreated	2403	141	DI water: 0.11	1080	0.58	0.21

*Liquid content = Mass of liquid/total mass of solids

$^{\downarrow}$Based on a particle density of 2.57 for this sand/lignocellulose composition

185 Clear acrylic columns with inner diameter of 100 mm and a total height of 550 mm
186 were used for incubation of the samples. A 50 mm thick layer of gravel was placed at
187 the bottom of the column followed by a layer of non-woven geotextile to prevent the
188 transport of soil particles into the gravel layer. The moist soil mixture was then
189 compacted in 9 equal layers in the column, with each layer tamped to form a final
190 sample of 300 mm length with an initial dry density of 1080 kg/m^3. Pre-drilled slots
191 for insertion of sensors on the column wall were sealed using foam plugs and cellotape
192 prior to emplacement of the soil. After compaction, the top of the column was covered
193 with a sheet of aluminium foil to reduce moisture loss and prevent contamination.
194 Samples were stored in an incubator at 25°C, in the dark, for 12 weeks to allow for
195 mycelium growth (i.e. fungal treatment) prior to testing.

196 In total, 4 samples comprising 2 treated and 2 untreated were prepared and incubated.
197 After incubation, one pair of columns (1 treated and 1 untreated) was sub-sampled (i.e.
198 cut to a smaller height) for soil water retention testing as described in section 3.1.3
199 and Figure 3. The second pair of untreated and treated columns were used for the
200 infiltration test (section 3.2.1) and then subsequently for the hydraulic conductivity
201 tests (section 3.2.2). The infiltration and hydraulic conductivity tests were conducted
202 on the full height of the incubated specimens (i.e. 300mm).

203 # 3 Experimental procedures

204 ## 3.1 Soil water retention behaviour

205 ### 3.1.1 Experimental set-up

206 The soil water retention behaviour for fungal treated and untreated soils during wetting
207 and drying cycles was determined using the hanging water column technique.
208 Negative pore water pressures were imposed in the soil specimen by controlling the
209 level of water in a burette connected to the base of the specimen, see Figure 3b
210 (Pagano, Tarantino and Magnanimo, 2018). The burette was raised and lowered in
211 steps to increase and decrease pore water pressure respectively. Volumetric water
212 content (θ) in the soil specimen was determined in two ways: (i) by determining the
213 final water content of the specimen at the end of the experiment (θ_f) and knowing the

change in mass of water (recorded via the balance) occurring along a wetting path ($\Delta\theta_{i,\ wetting}$) and/or occurring along a drying path ($\Delta\theta_{i,\ drying}$) between a given step *i* and the end of the test.

$$\theta_i = \theta_f + \Delta\theta_{i,drying} - \Delta\theta_{i,wetting} \quad (1)$$

and (ii) local measurement of θ at 50mm depth using an ML2x-type Theta Probe (Delta-T devices). Similarly pore water pressure (u_w) at equilibrium (static conditions) was determined in two ways: (i) by calculating the hydrostatic pore-water pressure imposed by the water level in the burette:

$$u_w = h_w \rho_w g \quad (2)$$

where h_w is distance of the water level relative to soil specimen mid-height, ($h_w$is positive when the water level is above the mid-height of the specimen, and negative when it is positioned below), ρ_w is the density of water and g is the acceleration due to gravity and (ii) local measurement at 50mm depth (specimen mid-height) using a T5x-5 pressure transducer tensiometer (5cm shaft length) from UMS Ltd.

The negative water column technique requires the use of a high air-entry filter at the base of the soil specimen to ensure that the negative pore water pressure applied is transferred to the specimen while ensuring the drainage system remains fully saturated. However, a silt filter was used in these experiments instead of the conventional porous stone because it prevents the build-up of larger pores at the interface between the specimen and the filter, a phenomenon known as the *wall effect* which occurs at interfacial boundaries of sands or coarse-grained materials (Pagano, Tarantino and Magnanimo, 2018). The silt filter used has an air-entry value greater than 10kPa (Pagano et al., 2019). The negative water column technique was first used to consolidate the silt filter and later used to impose the wetting and drying paths to investigate water retention behaviour.

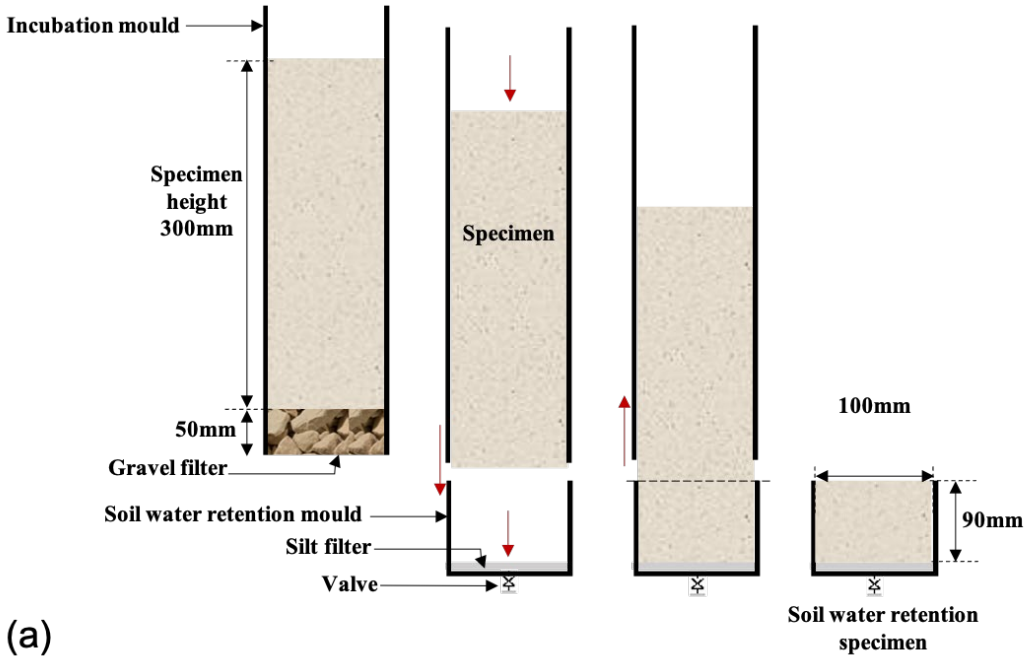

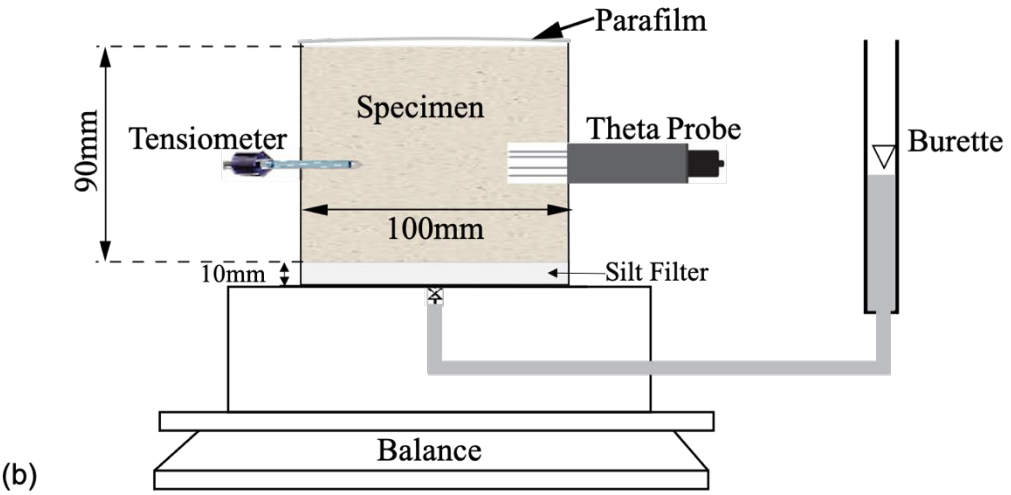

Figure 3. (a) Transfer of soil sample from incubation column into mould for water retention tests. (b) experimental set up for determination of the soil water retention curve for fungal treated and untreated sand

3.1.2 Preparation of the silt high air-entry filter

Silt, with a mean particle size of 25.2 µm produced from crushed quartz stone and commercially available as 'silica' was used for making the silt filter. A drainage pipe

250 with a valve (initially closed) connected to a burette was fixed to the bottom of the soil
251 water retention mould (see Figure 3). A 100 mm diameter filter paper was placed
252 inside the mould before gently pouring in the silt slurry prepared at water content,
253 w=100%. The filter paper was aimed to prevent flow of the slurry into the drainage
254 pipe. The slurry was left to settle for 48 hours. The height of water in the burette was
255 adjusted so that it was just several millimetres above the height of the silt filter and the
256 drainage valve opened to enable drainage of excess water (Pagano, Tarantino and
257 Magnanimo, 2018a).

258 Consolidation of the filter was achieved using the negative water column method. The
259 burette was lowered in discrete steps to achieve a pore water pressure of -7 kPa,
260 applied in steps of 1kPa. This value is associated with the minimum pore water
261 pressure imposed to the soil to characterise its water retention behaviour and therefore
262 ensured that the silt filter did not experience plastic deformation when the soil was
263 dried or wetted. Hydraulic equilibrium was targeted for the imposed pore-water
264 pressure, indicating consolidation of the filter. This was observed by recording the
265 change in water level of the burette and the mass of the silt filter determined from the
266 balance. At the end of the consolidation process, the silt filter had a final height of
267 10mm. The burette was then raised in steps until its water level was just above the
268 surface of the silt filter, imposing zero pore water pressure on the surface of the silt
269 filter. Given its preparation from a slurry state and that it has an air-entry value >10kPa
270 suction, the silt was assumed to be fully saturated at this stage.

271 **3.1.3 Emplacement of soil specimen**

272 The requirements to consolidate the silt filter and to ensure it remained fully saturated
273 throughout the experiment made it difficult to prepare the treated sample in the water
274 retention mould from the outset, as the silt filter would have lost moisture during the
275 fungal growth period (12 weeks) in the incubator. After emplacement of the silt filter,
276 samples were therefore transferred from the incubation mould (specimen height
277 300mm) into a shorter mould (specimen height 90mm) for the soil water retention tests
278 as shown in Figure 3a. The bottom of the column bearing the 300 mm sample was
279 removed and the gravel filter taken out. Using a pusher that fitted tightly within the

column, the sample was carefully pushed until it was flush with the base of the column. The column was then placed on to the water retention mould containing the consolidated silt filter, perfectly aligned. With the pusher and guided by linear scale and reference marks attached to the column, a 90 mm thick specimen was pushed into the mould and the top neatly cut using a wire hand saw. One tensiometer for monitoring pore water pressure (in the positive and negative ranges) and one ThetaProbe for measuring volumetric water content were then installed at 50 mm depth for determination of the soil water retention curves (Figure 3b). After emplacement the specimens had values of pore water pressure and volumetric water content (from sensor measurements) of -2kPa and 15.40% for the untreated specimen and -4.9kPa and 16.98% for the treated specimen.

3.1.4 Wetting and drying procedure

First wetting was achieved by raising the level of water in the burette in steps, from just above the top of the silt filter until it reached the same level as the top of the specimen, imposing zero pore water pressure at the top of the specimen. After each water level change, hydrostatic equilibrium was reached before increasing the water level. Equilibrium was indicated by no further change in mass recorded by the balance. After the first saturation (wetting), the water level in the burette was then lowered in stages to impose decreasing values of pore-water pressure along the drying path. The same processes were repeated to achieve the second wetting and second drying cycle.

3.1.5 Sensor data quality check and calibration

Soil water retention curves are presented in this study in terms of local measurements at a soil depth of 50mm. In order to check the response of the T5x tensiometer, the pore-water pressure measured by the tensiometer was compared to the one imposed by the water level in the burette at equilibrium. This comparison is presented in Figures 4a and b for the untreated and treated specimens respectively and indicates a satisfactory response of the tensiometer sensor. Figure 4b also confirms that in the case of the fungal treated specimen that the negative pore-water pressure imposed by the hanging-column method could be transmitted to the soil specimen.

309 Given that the soil mixture is a non-typical soil composition containing lignocellulose,
310 the ThetaProbe measurements of volumetric water content were directly calibrated
311 based on the global volumetric water content determined for the untreated and treated
312 specimens. The water content values returned by the ThetaProbe based on the default
313 manufacturer calibration were treated as raw data and the parameters of a linear
314 calibration were determined by best-fitting of the volumetric water content data
315 derived from balance measurements. These parameters are reported in Table 2 and
316 illustrate that the presence of fungal mycelium does influence the bulk dielectric
317 permittivity. Figures 4c and d show the quality of the calibration established for the
318 untreated and treated soil. The same calibration was applied to the ThetaProbe
319 measurements of volumetric water content obtained during the ponded infiltration test.

320
321 *Table 2: Thetaprobe calibration parameters for untreated and treated soil*

Specimen	Intercept	Slope
Untreated	3.67	1.17
Treated	10.05	0.81

322

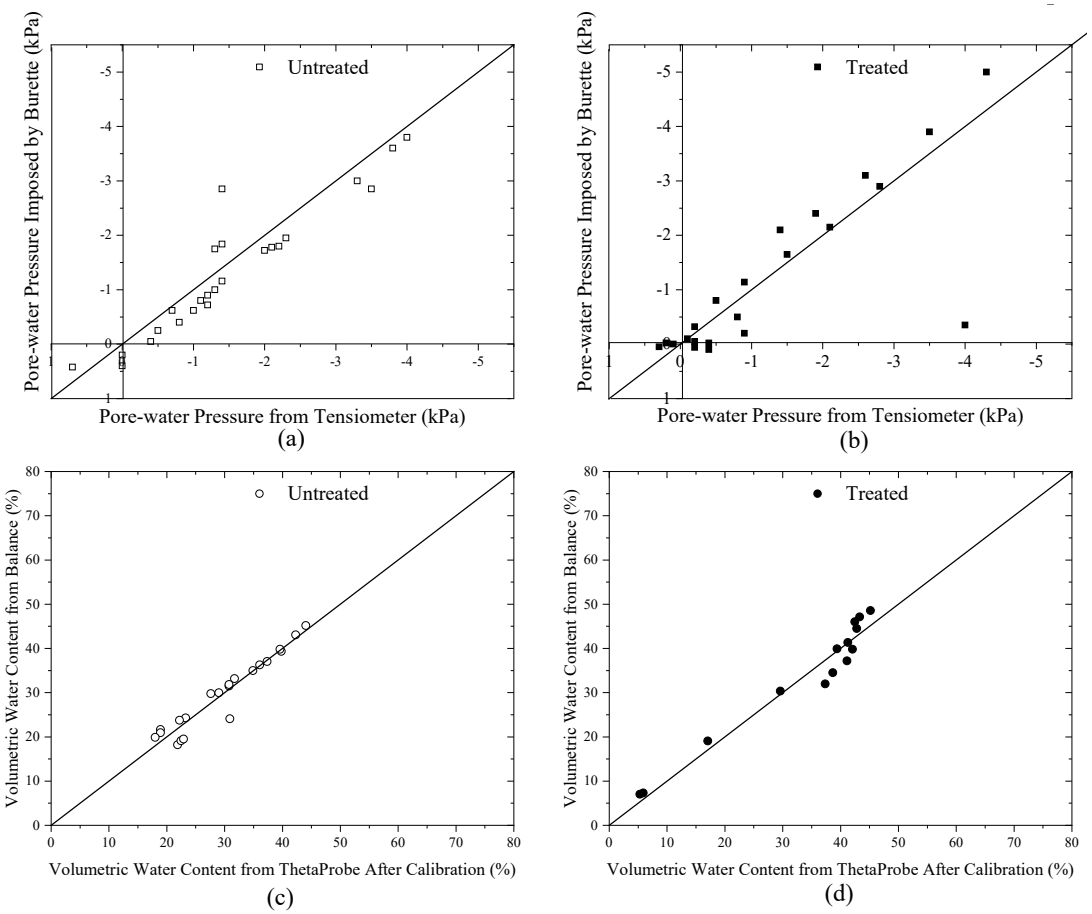

Figure 4. Comparison of (a and b) pore-water pressure imposed by water level in burette with pore-water measurements from tensiometer and (c and d) volumetric water contents determined from balance measurements and ThetaProbe for untreated (left: a & c) and treated (right: b & d) specimens.

3.2 Ponded infiltration and quasi-saturated hydraulic conductivity tests

3.2.1 Ponded infiltration test

After 12 weeks of growth, the second pair of samples were taken out of the incubator and set up directly for infiltration testing (Fig. 5). The sensors were inserted through the pre-drilled slots into the specimen, and silicon sealant was used to ensure a water-tight installation. The column was then left overnight to allow the silicon sealant to dry and for the sensors to equalise. The volumetric water content at this stage was ~10% for the untreated specimen and ~18% for the treated specimen. The infiltration test was carried out by applying a constant head of water (25 mm) at the specimen surface. A sheet of non-woven geotextile material was placed on the surface of the specimen at the soil-water boundary in order to minimise soil disturbance while setting

the constant head. The wetting front and corresponding transient pore-water pressures were monitored using the ThetaProbes and tensiometers, a pair of each were installed at depths of 25, 150 and 275 mm (see Figure 5). Pore-air migrated upwards through the column during infiltration and also via the outlet at the base of the column. The time at which water infiltration commenced and the time when outflow started at the bottom of the column were both recorded. Shortly after steady state flow conditions were achieved (monitored via the balance measurements), inflow was stopped and the specimen was allowed to drain by gravity.

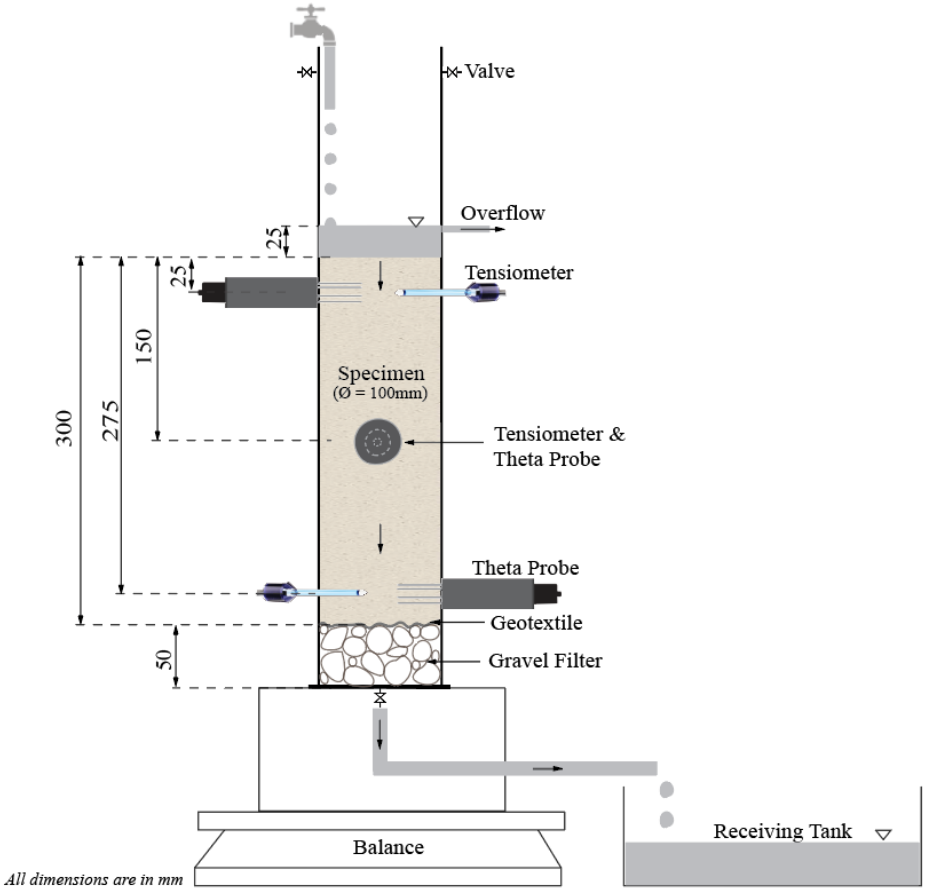

Figure 5. Set-up of 1D infiltration column instrumented with tensiometers and ThetaProbe sensors connected to a data logger.

3.2.2 Quasi-saturated hydraulic conductivity test

Immediately after the infiltration test, the same specimen was then used for determination of the quasi-saturated hydraulic conductivity (k_s) of the soil by

conducting constant head permeability tests (ASTM D5084-10). The specimens were initially quasi-saturated by raising the reservoir upwards gradually in steps until level with the surface of the specimen. For the untreated specimen, a degree of saturation of $S_r = 0.98$ was achieved after 4hrs whereas it took ~3 days to attain $S_r = 0.86$ for the treated specimen. k_s (at 20°C) was determined in conditions of upward and downward flow through the specimen (as illustrated in Fig. 6) according to Darcy's law:

$$Q = Ak_s i \quad (3)$$

where A is the cross-sectional area of the specimen, i is the hydraulic gradient applied across the specimen, and Q the flow rate.

Since the hydraulic conductivity test was carried out at pore-water pressures close to or slightly greater than zero (up to 6 kPa), this test characterises the quasi-saturated hydraulic conductivity or the field-saturated hydraulic conductivity (Nimmo *et al.,* 2009), which is when the soil has been brought to a near-saturated state by water applied abundantly at the land surface, typically via rainfall or irrigation. This type of wetting usually traps air in a significant fraction of the pores, and as such the hydraulic conductivity is less than the conductivity in a totally saturated state which may be achieved by artificial means. It is relevant in problems such as rainfall-induced landslide hazard which fungal-treatment has potential to mitigate.

For all the experimental set-ups described in sections 3.2.1 & 3.2.2, an advanced data logger and controller (GP2 from Delta-T devices) with *Deltalink 3.6.2* software was used for acquisition and logging of data from the respective sensors, while the mass readings from the balance were continuously recorded via a serial port using *Tera Term*, an open-source programme.

3.3 X-ray Micro-Computed Tomography scanning

In order to better understand the influence of fungal treatment on soil microstructure, specimens were scanned using X-ray Micro-Computed Tomography (X-μCT). Untreated and treated specimens were prepared in accordance with the ratios of sand, lignocellulose, DI water/fungal suspension presented in Table 1. The untreated specimen was scanned 1 week after preparation. The treated specimen was scanned

16 months after preparation. Immediately after inoculation with the fungal suspension the treated specimen was incubated for 3 weeks in the dark at 25 ºC, after which it was fully saturated, thereafter it was stored at 20±1ºC and RH = 40±5%. Although the time after inoculation (16 months) is much greater for the X-μCT scanned treated specimen than the time at which the water retention, ponded infiltration and hydraulic conductivity behaviour was investigated (3 months), these scans still give a useful qualitative insight into the evolution of the microstructure with fungal treatment.

The untreated and treated specimens were scanned in 3D using a Nikon Metrology X-μCT system with 180 kV X-ray transmission target. Relevant X-ray acquisition settings were: 120 kV, 33 μA, 1415 millisecond exposure, and 3142 projections at 0.1146° angular intervals resulting in a total scan time of 1 hour 15 minutes. The scans were reconstructed into a 3D dataset consisting of a series of 16-bit 2D slices with a resolution of 5.52 μm for the treated sample, and 4.66 μm for the slightly smaller untreated sample. In this dataset the X-ray attenuation (represented by the grayscale value) is approximately equal to the sample density hence air-filled pores have the lowest attenuation, sand grains have the highest attenuation. Lignocellulose, fungal mycelium biomass and water have similar grayscale values which lie between that of air and sand.

Image processing of the 3D dataset was performed with the FIJI distribution of ImageJ (Schindelin *et al.*, 2015) and consisted of cropping the central section of each scan to a 5x5x5 mm cube, then applying the Trainable Weka machine learning tool (Arganda-Carreras *et al.*, 2017) to segment the scan into three phases: pore space, sand grains, and combined lignocellulose/fungal mycelium/residual water. Given the similar density of lignocellulose, and thus the lack of x-ray attenuation contrast between fungal mycelium and water, it was not possible to segment these phases separately using the Nikon Metrology X-μCT system at Strathclyde.

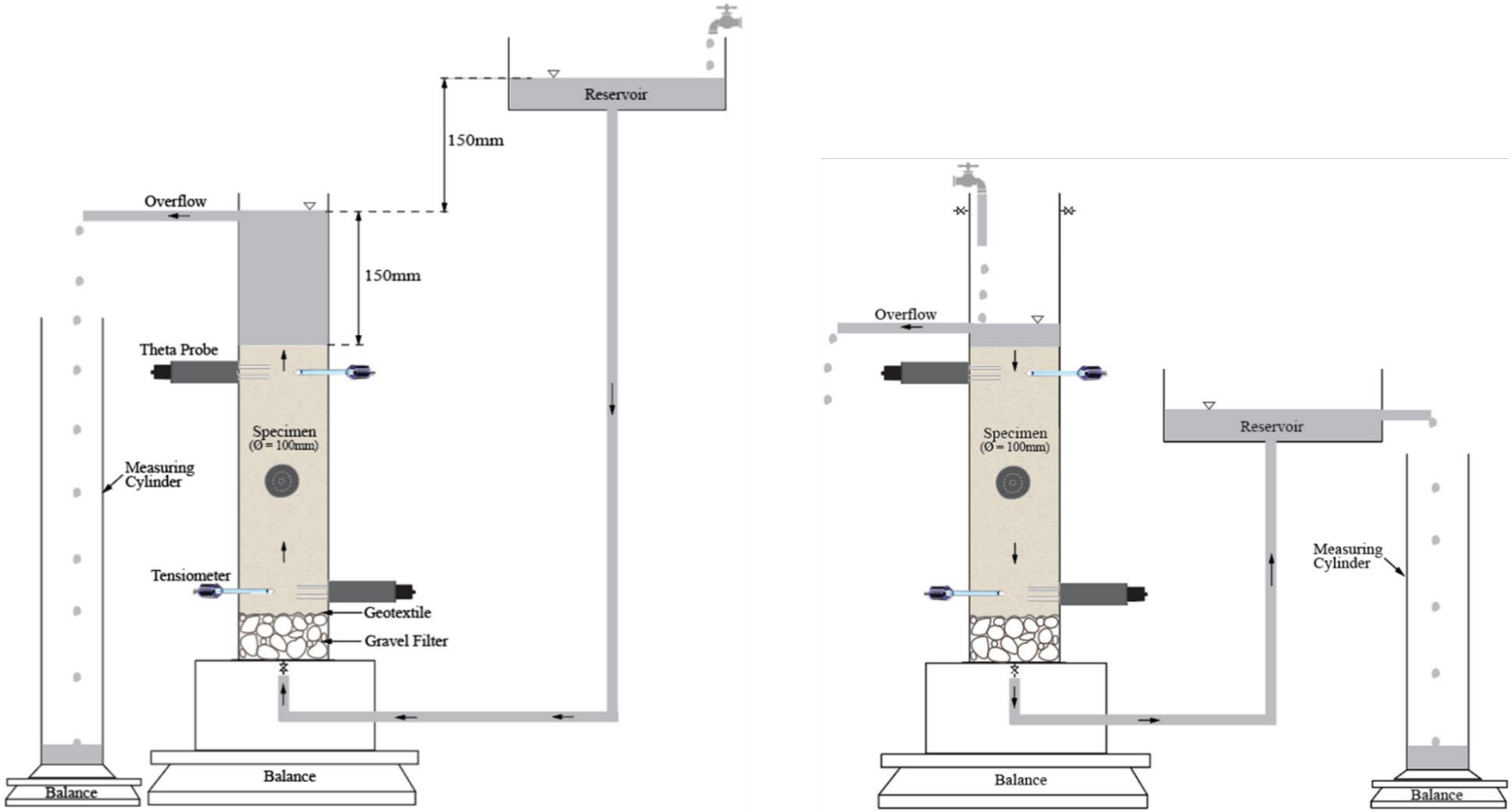

Figure 6. Determination of k_s via upward flow (left) and downward flow (right)

4 Results

4.1 Soil water retention behaviour

Figure 7 presents the soil water retention curves based on the measurements obtained via the tensiometer and ThetaProbe at a depth of 50mm (specimen mid-height) for the untreated and treated specimens respectively during the first and second wetting-drying cycles.

It should be noted that the base of the specimen was connected to a burette as shown in Figure 3b. To impose a drying path for example, the level of water in the burette was decreased. As water flowed from the specimen to the burette, the water level in the burette increased a little until static equilibrium was eventually established. The values of pore-water pressure imposed by the water level in the burette under conditions of static equilibrium were therefore variable because they depended on the amount of water that flowed from the specimen into the burette. Figure 7 shows the static equilibrium data points as solid symbols and the data points derived from the sensor readings (tensiometer and Theta Probe) acquired during the transient stage with open symbols. The water retention data acquired under transient and static conditions are very consistent and were both used to characterise the drying and wetting water retention curves. The water retention curves are drawn manually to facilitate the reading of the plot.

The untreated specimen undergoes gradual first wetting with a water-entry value between -1 and -2 kPa pore-water pressure and gradual first drying with an air-entry value at around -1 kPa pore-water pressure, which is consistent with the behaviour of sand (Pagano, Tarantino and Magnanimo, 2018b) (Figure 7a). As expected, the second wetting and drying paths follow the first wetting and drying paths. The maximum water content reached at a pore-water pressure of 0.7 kPa along the first wetting path is close to the porosity measured independently (n=0.56, note this is lower than the initial specimen porosity (Table 1) due to volumetric collapse of the untreated specimen during wetting). This indicates that the specimen was close to saturation (S_r=0.94) at the end of the first wetting path. In the untreated specimen, the ink bottle effect, the raindrop effect and air entrapment during wetting via capillary rise are likely to have contributed to the S_r<1 that was achieved (by imposing a very small positive pore-water pressure) and also the hydraulic hysteresis observed. This means that for a given negative pore-water pressure, the untreated specimen exhibited significantly different volumetric water content depending on whether it was on a wetting curve or a drying curve.

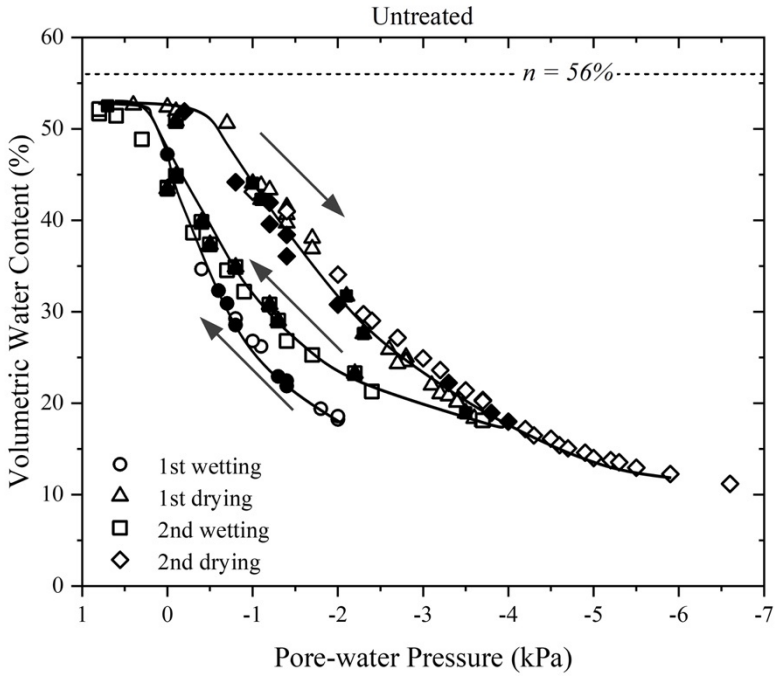

(a)

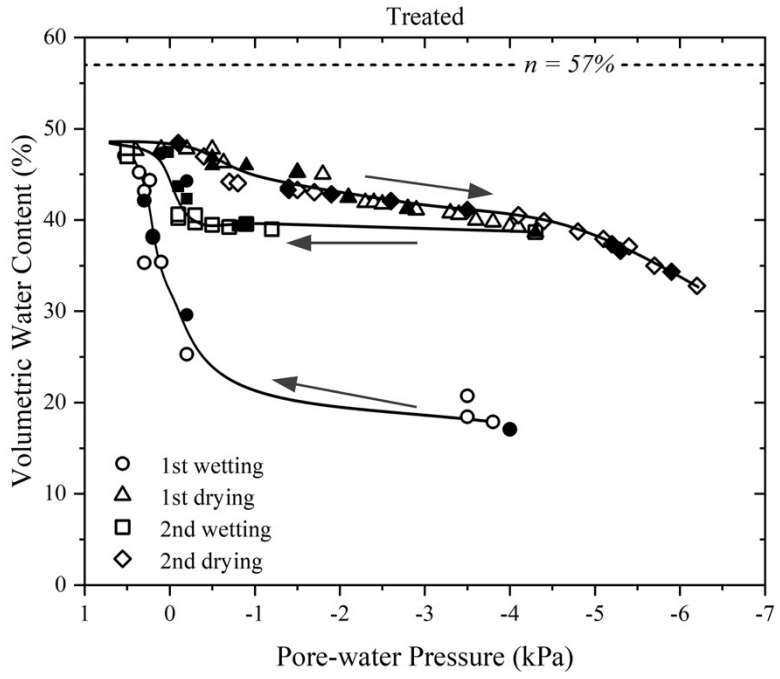

(b)

Figure 7. Soil water retention curves for the (a) untreated and (b) treated specimens. Open symbols refer to data points acquired during transient stage, solid symbols refer to data point associated with static equilibrium. Water retention curves are drawn manually.

In contrast to the untreated sand, the wetting curves of the treated specimens exhibit an on/off pattern, i.e. the water content increases sharply once the pore-water pressure increases above

451 the water-entry value. Along the first wetting path, there is little variation in water content over
452 a relatively large range of (negative) pore-water pressures before the water content increases
453 sharply at around -0.5kPa (water-entry value) (Figure 7b). At slightly positive pore-water
454 pressure, the volumetric water content remains significantly lower than the porosity, with a
455 degree of saturation S_r~0.85. This relatively low degree of saturation is associated with infilling
456 of pores with fungal biomass. Water content decreases very gently along the drying paths and
457 a sharp decrease in volumetric water content (i.e. the air-entry value along the drying scanning
458 path) of the treated specimen is not captured within the pore-water pressure range tested (up to
459 -6kPa). This indicates that the air-entry value has been shifted to a lower value of pore-water
460 pressure (i.e. higher suction) due to fungal treatment and growth. It is evident that there is much
461 greater hydraulic hysteresis in the treated specimen, particularly between the first wetting path
462 and drying curves.

463 The changes in water retention behaviour are associated with a change in pore-size distribution
464 as also highlighted by the times required for equalisation to be reached after each change to the
465 imposed pore-water pressure (i.e. level of the water in burette). The two wetting and drying
466 cycles on the untreated specimen took 19 days to complete whereas it took 48 days to complete
467 the test on the treated specimen.

468 **4.2 Ponded infiltration behaviour**

469 Figure 8 presents the evolution of volumetric water content and pore water pressure with time
470 from the start of infiltration for both the untreated (U) and treated (T) specimens at depths of
471 150mm (a, b) and 275mm (c and d). The readings recorded by the topmost sensors (at depth of
472 25mm) are not presented because due to volumetric collapse of the untreated specimen
473 (described below) the sensors were immersed in water after t= 6 mins rather than being
474 embedded within the soil (see Fig 9aiii). Hence, the readings were not considered relevant for
475 comparison with the treated specimen at the same depth.

476 From Figure 8a & b, it can be seen that the infiltration front for the untreated specimen reached
477 the sensors at a depth of 150 mm at t ≅ 2mins leading to an increase in volumetric water content
478 θ from ~10% to 61% and u_w from -8.4 to 2.2 kPa within 3 mins. θ increased further to 76% by
479 the 6th minute before stabilising at ~ 64% by the 30th minute, while u_w stabilised at ~1.1kPa
480 from t = 30mins. Based on the post-collapse porosity, a saturated volumetric water content of
481 ~52% was expected, however that assumes a uniform density is achieved throughout the

column after volumetric collapse, which appears not to have been the case. The very high volumetric water contents ~76% temporarily observed between 3-30mins are likely due to an expansion of the porosity within the middle section of the specimen temporarily, as volumetric collapse of the lower portion of the column occurred while the upper portion of the column was sustained by lateral friction.

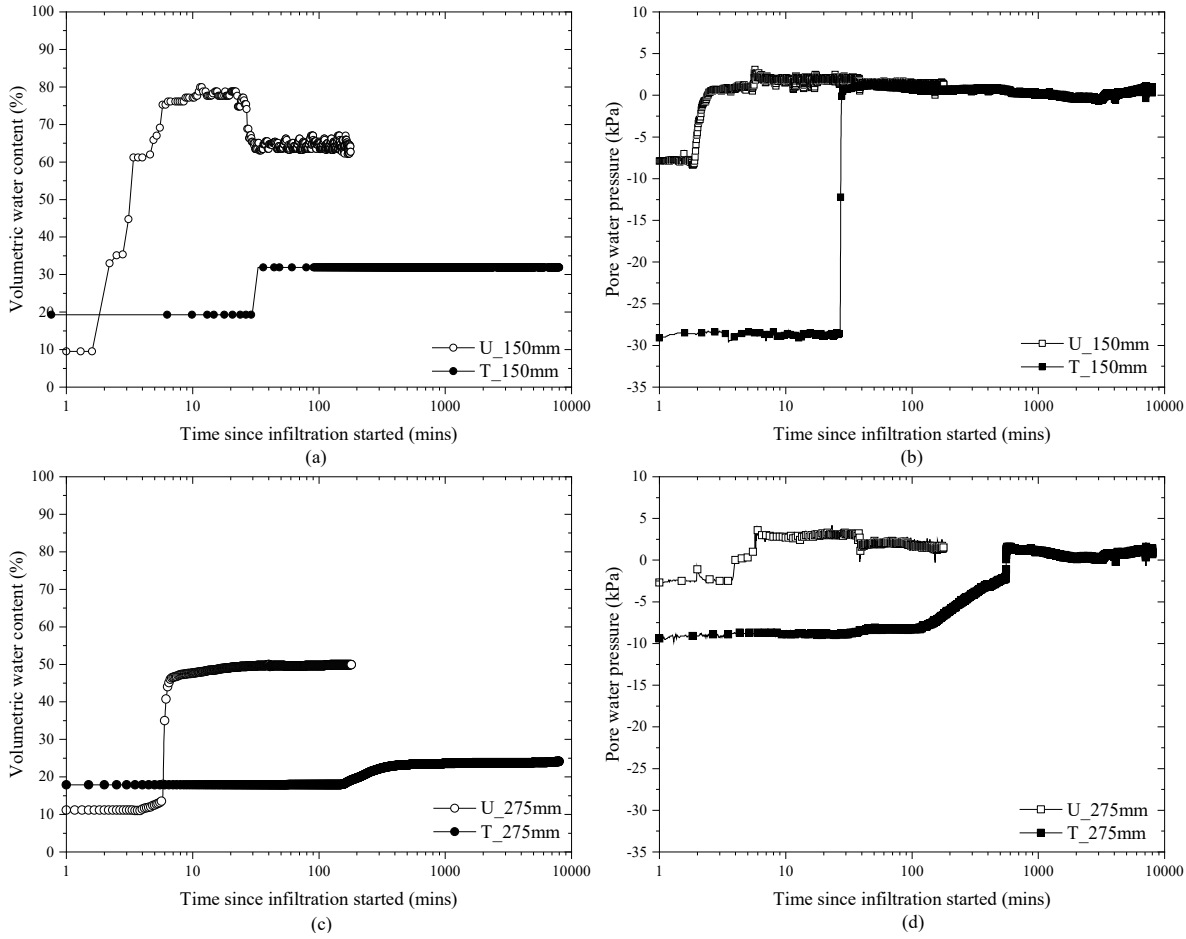

Figure 8. Evolution of volumetric water content (a & c) and pore water pressure (b & d) with time for the untreated (U) and treated (T) specimens during infiltration recorded at depths of 150mm (a & b) and 275mm (c & d).

For the treated specimen, water did not reach a depth of 150mm until t ≅ 31 mins; this resulted in an increase in θ from 19% to 32.5% within 2 minutes (Fig 8a). Thereafter θ remained stable at 32.5%, and did not reach saturation (where $\theta_{sat} \approx 57\%$) throughout the remaining ~8000 minutes (5.5 days) of the test. Similarly, at t ~30 mins, u_w in the treated specimen increased from -28.5kPa to ~1.8kPa (Fig 8b).

It is evident in Figures 8c & d, that the wetting front in the untreated specimen reached both sensors at the depth of 275mm at t ~ 4 mins, reaching a volumetric water content of 50% (Sr =

0.89). Whereas for the treated specimen, changes in θ were not recorded until t = 168 mins and even by the end of the test (after 5.5 days of continuous infiltration) the saturated volumetric water content (of 57%) was not reached. A small increase in u_w was observed to occur after t = 37 minutes, and a gradual steady increase from t = 127 mins, with all suction lost (u_w = 0kPa) at t = 540 mins. This highlights that infiltration into the treated specimen was much slower than for the untreated specimen. The fact that unsaturated conditions prevail at a depth of 275mm, while pore water pressure values are positive (after t = 540 mins) indicates that infiltration in the treated specimen does not occur via a uniformly advancing wetting front (this is discussed further below).

Figure 9 shows images captured during infiltration for the untreated and treated specimens between 0 – 60 mins and 0 – 200 mins respectively. At 3 mins after infiltration commenced, the untreated specimen had undergone volumetric collapse with the initial surface level lowered by ~20mm (Figure 9aii). The observed collapse/densification occurred because air in the pore spaces of the initially loose sand specimen (at a dry density of 1.08 g cm^{-3}) were displaced by water as infiltration progressed, as such, there was a loss of water menisci at grain contacts, which were providing a stabilising effect in this loose specimen (i.e. volumetric collapse on wetting, e.g. Barden, *et al.,* 1973). The low density of the specimens was selected in order to ensure adequate aeration for fungal growth. At t = 3 mins, the uniformly advancing wetting front in the untreated specimen had reached a depth of 230mm, and reached the base of the untreated specimen by t = 6 mins. At this stage, a further 10mm lowering of the specimen surface level was recorded and both sensors at a depth of 25mm now protruded above the soil. By t = 60 mins, steady-state conditions had been established (indicated by no change in the mass recorded on the balance below the specimen) and no further densification occurred. These conditions were maintained until t = 100 mins when the test was terminated.

For the treated specimen, evidence of mycelium growth and specimen colonisation was visible in the form of white colouration and mycelial cords in the specimen (see Fig 9bi). At t = 3 mins, a uniform wetting front had reached a depth of only 40mm (Fig 9bii) compared to 230mm depth at this time for the untreated specimen). No further advance in infiltration was observed until t=30mins, after which the initiation of preferential flow in the form of fingering was observed (see Fig 9biii). By t= 200 mins, preferential flow paths extended to the base of the specimen (Fig 9biv). A volumetric collapse of only 1% (change in height/initial height)

occurred in the fungal treated specimen during infiltration compared to a volumetric collapse of 10% that occurred during in the untreated specimen.

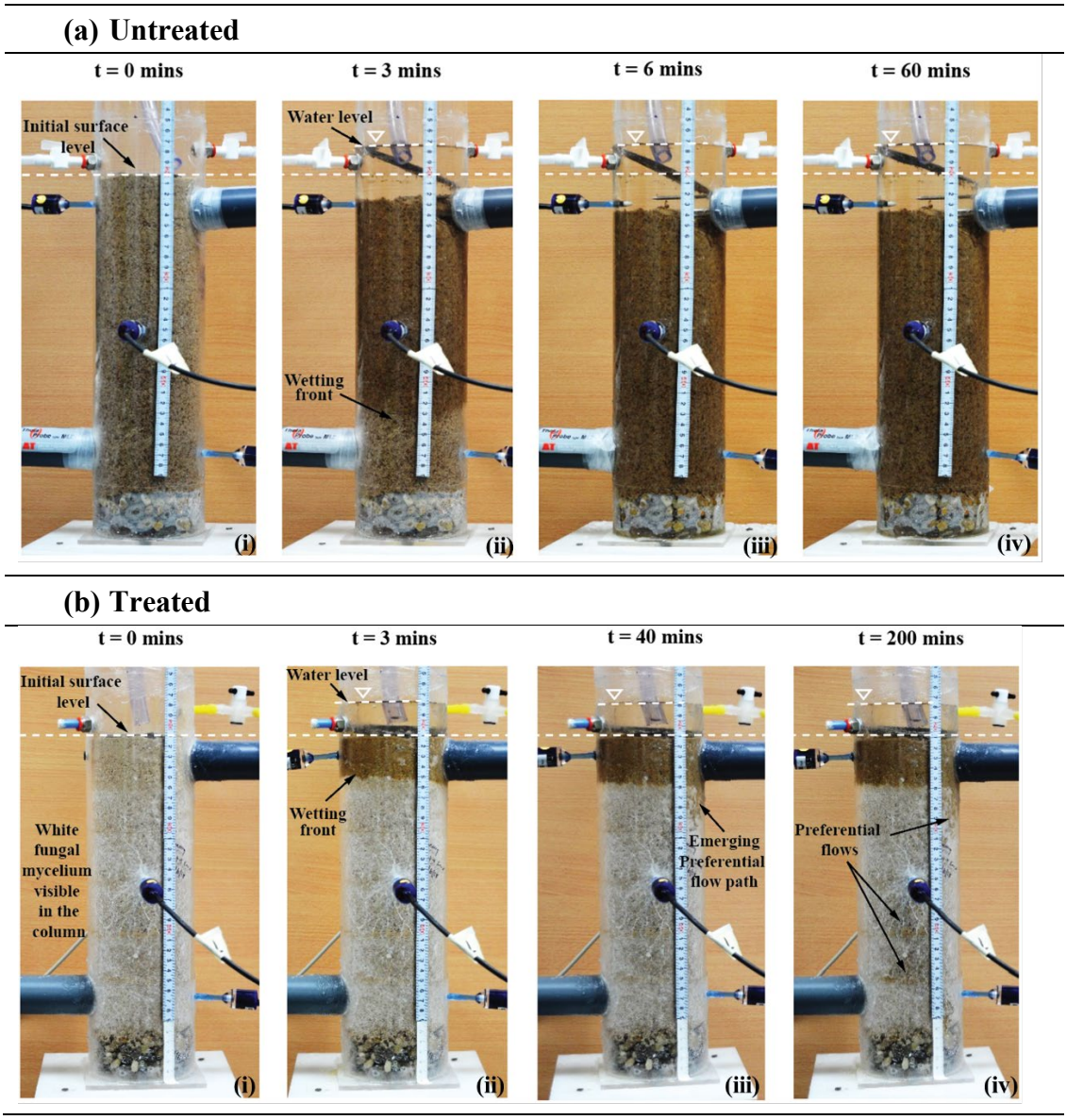

Figure 9. Time lapse photography of infiltration into (a) untreated and (b) treated specimens.

In summary, the wetting front in the untreated, advanced uniformly, as expected for a sand and reached the bottom of the specimen, within 6 minutes. In the treated specimen, the wetting front initially advanced uniformly, to d ~40mm within the first 3 minutes of the test, thereafter infiltration was delayed, before infiltration proceeded via preferential flow paths with sensors at d = 150mm responding in the range of t = 31-33 mins and at d = 275mm responding in the range of t = 130 – 168 mins. The clear change in flow regime below a depth of 40mm indicates that fungal biomass was more developed in the sand below this depth significantly altering the hydraulic behaviour of the sand.

4.3 Quasi-saturated hydraulic conductivity

Quasi-saturated hydraulic conductivity was determined for both specimens by downward and upward flows. Figure 10 presents the discharge per unit area (flux) against hydraulic gradient for the untreated and treated specimens. Linear regression lines were fitted to the data points to obtain the respective quasi-saturated hydraulic conductivities k_s. The average k_s for the untreated specimen determined from both downward and upward flows was found to be ~ 1.34 x 10^{-4} m s^{-1} while for the treated specimen it ranged between 3.1 x 10^{-5} to 5.2 x 10^{-5} m s^{-1}. The results show that fungal treatment with *P. ostreatus* can reduce the quasi-saturated hydraulic conductivity of a sand by up to one order of magnitude.

The difference in k_s can be partly attributed to the different degrees of saturation achieved in the untreated and treated sand columns after submersion with water (S_r=0.98 and 0.86 for untreated and treated respectively). Also, the difference in quasi-saturated hydraulic conductivity of the treated specimen between upward and downward flow can be possibly explained in terms of different levels of saturation achieved. The pore-water pressures imposed in the upward flow test Figure 6 (left) are higher than those imposed on the downward flow test Figure 6 (right). This would have generated a slightly higher degree of saturation resulting in a slightly higher quasi-saturated hydraulic conductivity. Higher volumetric water contents were indeed measured in the treated specimen during measurement of k_s in the upwards flow condition compared to the downwards flow condition (e.g. 48.6% and 46.72% respectively at a depth of 275mm).

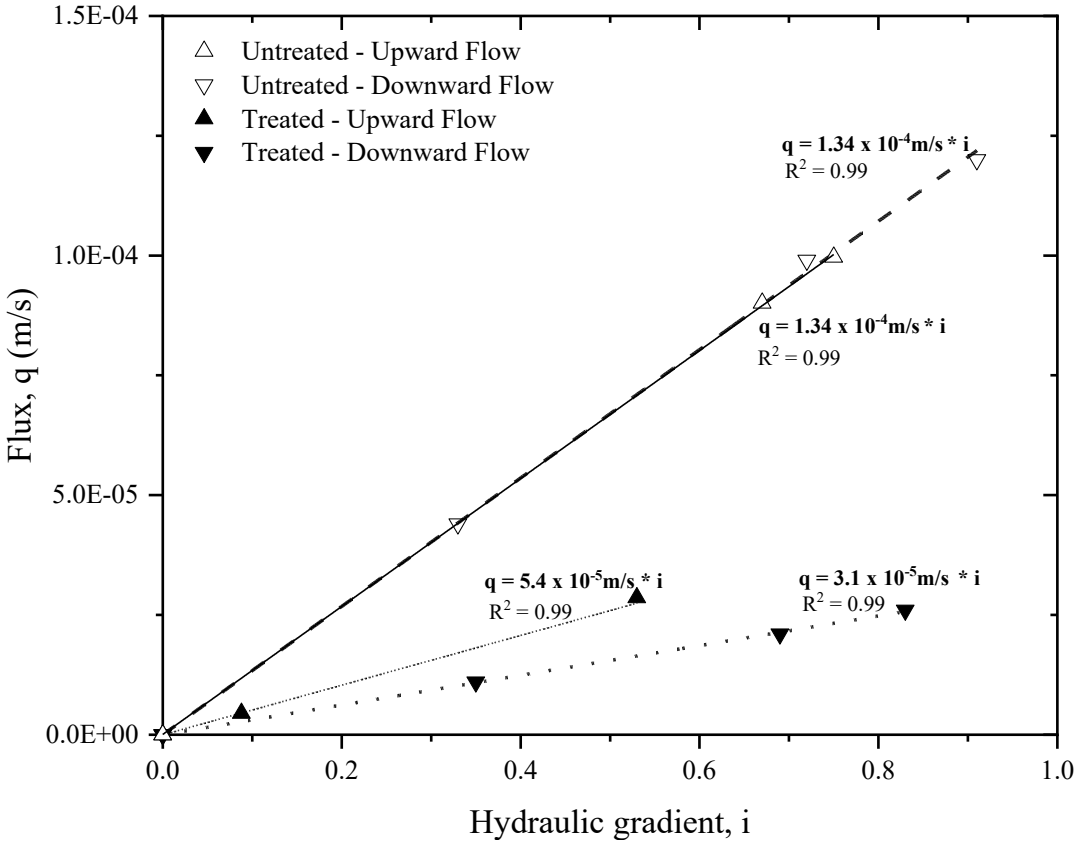

560

561 *Figure 10. Plot of flow per area vs hydraulic gradient for upward and downward flows in treated and untreated*
562 *specimens*

563 **4.4 Microstructural observations via X-µCT**

564 Figure 11 shows cropped sub-sections from scans of an untreated specimen (a – b) and treated
565 specimen (c – h). Using the Trainable Weka machine learning tool, the 3-phase segmentation
566 achieved are presented as pore space, sand grains and combined lignocellulose/residual water
567 (as in Figure 11b) or lignocellulose/fungal mycelium/residual water (as in Figure 11d, f & h).

568 For the untreated specimen (Figure 11a & b), it can be clearly seen that the sand grains appear
569 loose and discrete, neither bound nor connected together by any phase. It is also clear from
570 Figure 11 that the lignocellulose in the untreated specimen is angular in shape and exists as
571 discrete objects separate from the sand grains.

572 In the treated specimen, it was not possible to segment separately between
573 lignocellulose/fungal mycelium based on a lack of x-ray attenuation contrast (i.e. the materials
574 are of similar low density). However, they can be differentiated to an extent based on
575 morphology by comparison with the detected lignocellulose in the untreated specimen (Fig 11

a & b). It is evident that some of the areas highlighted in green (e.g. Fig 11f bottom left) resemble the morphology of lignocellulose (angular, large shapes) however from their edges extends finer material. As the fungi use the lignocellulose as their carbon source, they digest this material and mycelium growth appears to originate and extend from the lignocellulose substrate in a less discrete and less angular form (centre of Fig 11f). Whereas in Fig 11h, the morphology of the area highlighted in green does not resemble that of lignocellulose (as shown in 11a & b) and is attributed to fungal mycelium growth.

In the treated specimen, varying levels of fungal effects are observed. In Figure 11c & d, there are some small localised patches of fungal mycelium observed between two or three sand grains, but on the whole much of the sand grain surfaces in Fig11d appear to remain untouched by fungal mycelium. Whereas in Figure 11e & f, sand grains appear to be bound together and connected by interlinked patches of the combined lignocellulose/fungal mycelium phase. The fungal mycelium growth acts to both coat grain surfaces and enhance grain aggregation as seen in Figure 11f. Whereas, in Figure 11g & h extensive patches of fungal biomass have formed within the pores between sand grains, this growth has contributed to reducing the sizes of some of the pores within the treated soil compared to the untreated soil and clogging some pores entirely.

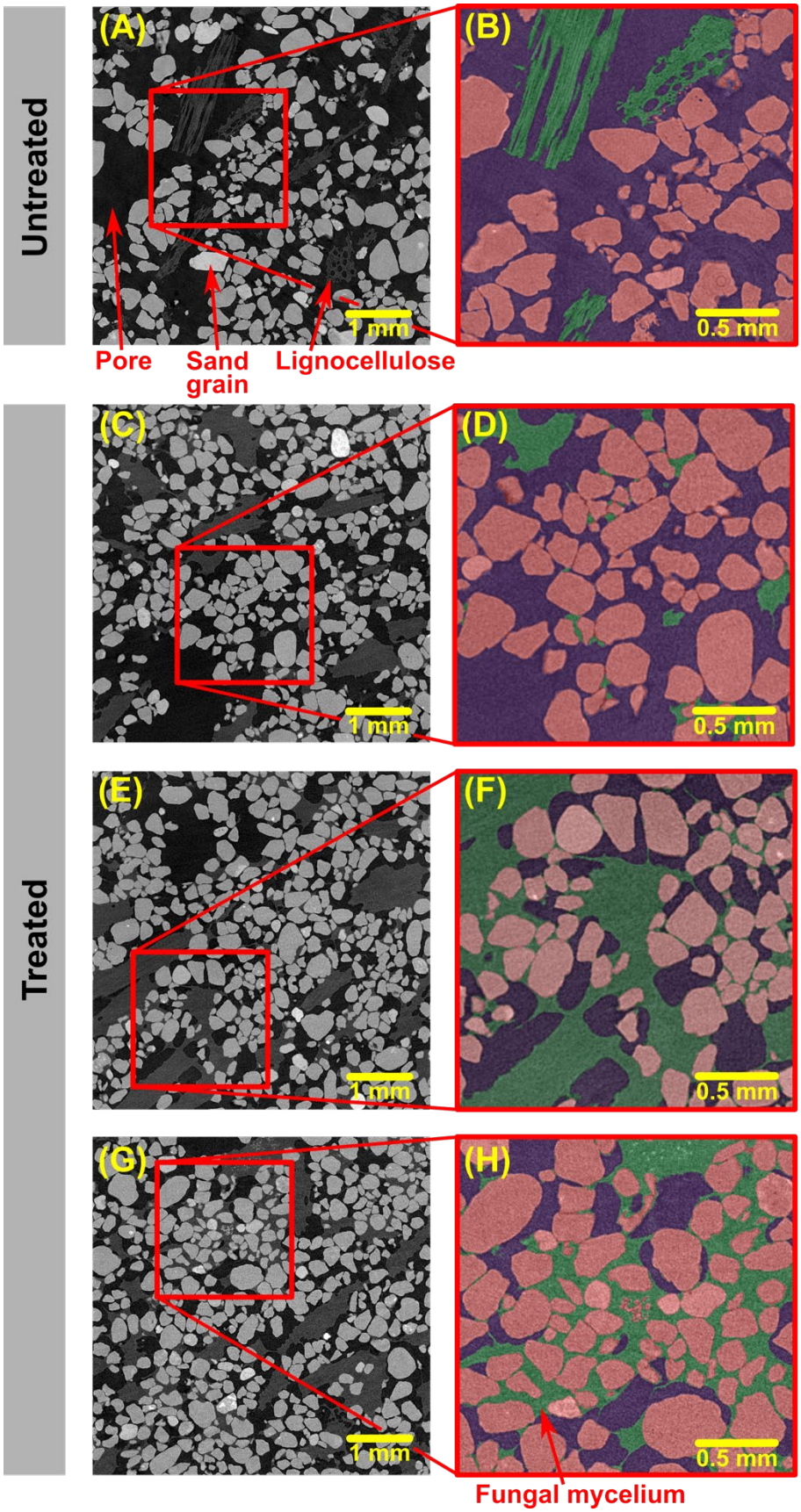

593

594 *Figure 11. Sub-sections of reconstructed 3D images of untreated (a – b) and treated (c – h) specimens obtained*
595 *from x-ray microcomputed tomography scanning*

5 Discussion

5.1 Biochemcial effects of fungal growth on pore network

P. ostreatus (and likely all filamentous fungi) produce hydrophobins, proteins which make fungi capable of hydrophobising hitherto hydrophilic surfaces and vice-versa (Wessels *et al.*, 1991; Wessels, 1996, 2000; Wösten, 2001). Salifu and El Mountassir (2020) demonstrated that after 12 weeks of growth of *P.ostreatus* in a sand (same soil and nutrient composition, sample preparation and growth conditions as used in this study) resulted in macroscopic liquid-solid contact angles of ~105° as measured at the specimen surface using the modified sessile drop method. The results in this study show however that not all the pores within a fungal treated specimen become hydrophobic. If all pores within the treated specimen became hydrophobic then it would not have been possible to transmit negative pore water pressures to the specimen using the hanging-column technique. Figure 4b demonstrates that the negative pore water pressure imposed by the hanging-column technique was indeed transmitted to the soil specimen, and there was good agreement between the tensiometer measurements and the values imposed by the hanging-column. Inspection of the images obtained via X-μCT (Figure 11) shows that fungal growth does not result in uniform treatment throughout the specimen, despite initial mixing of the fungal spore suspension with the sand/lignocellulose mixture. Indeed, in some regions the pores remained relatively unaffected by the fungal growth, in other regions mycelium is observed to bind grains together and coat grain surfaces, whereas other regions exhibited extensive biomass growth infilling pore space. Together, these results suggest that within a fungal treated soil there can coexist a continuous network of hydrophilic pores and a continuous network of hydrophobic pores. It is the hydrophilic water-filled pore-network that allows for the transmission of pore-water tension imposed by the hanging water column and measured by the tensiometer. Whereas the hydrophobic pore network is not invaded by water and remains air-filled (as water cannot rise into these hydrophobic pores from the water in the burette). Figure 12 presents the capillary analogue for the pore networks in an untreated specimen compared with the pore networks in a fungal treated specimen. The coexistence of air-filled and water filled continuous networks is commonly observed in (untreated) unsaturated soils. In the suction range between the air-entry suction and the residual suction, pore-air and pore water are both continuous in the pore space and any change of air pressure or water pressure at the sample boundaries can be transmitted through the sample.

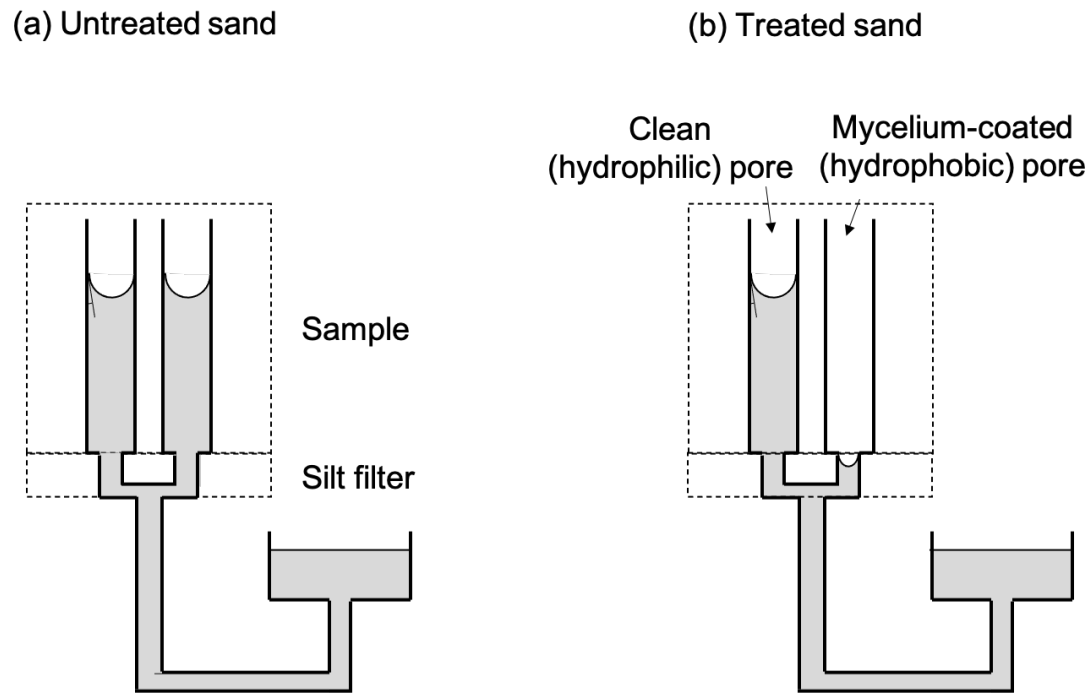

Figure 12. Capillary analogue of pore networks in (a) Untreated and (b) Fungal treated sand.

5.2 Biophysical effects of fungal growth on pore network

The growth of fungal mycelium also alters the physical structure of the pore-network. The microstructural analysis has indicated that as lignocellulose is digested fungal biomass is infilling pores and can contribute to reducing the number of pores available for water movement, as well as reduce pore diameter. Both the changes to the liquid-soil contact angle in some of the pores resulting from fungal produced hydrophobins (Salifu & El Mountassir, 2020) and these physical changes to the microstructure contribute to the alterations to the wetting and drying curves observed: (i) the steep gradients of the wetting curves once water advancement into the pores is initiated, (ii) the reduction in the size of some of the pores requiring higher suctions (i.e. more negative pore water pressures) to drain water from the fungal treated specimen compared to the untreated specimen along the drying paths and (iii) the increase in hysteresis between wetting and drying curves. This is consistent with literature that has demonstrated increasing hydraulic hysteresis in soils with an increasing percentage of artificially created hydrophobic particles (Orozco and Caicedo, 2017). The combined effects of the hydrophobic nature of some of the sand grain surfaces and the reduction in the size and frequency of the smaller pores contributes to the delay to infiltration, the development of preferential flow paths within the fungal treated soil, and the reduction in the quasi-saturated hydraulic conductivity measured. Similar behaviour including a delay in infiltration and the

development of preferential flow paths has been observed for sands treated with hydrophobic compounds (e.g. Wang, Wu and Wu, 2000).

Our findings are in contrast with results from other studies which have reported increases in infiltration and higher hydraulic conductivity (Crawford *et al.*, 2012; Pajor, 2012) in soils with fungi present compared to soils with no fungal growth. The main difference is that those studies were all carried out in silty/clayey soils where fungal growth enhanced the formation of aggregates and subsequent creation of macropores, thus increasing porosity and pore connectivity (Crawford *et al.*, 2012), whereas in sand our study has demonstrated that fungal growth contributes to pore filling.

5.3 Limitations of study

As a biological process, fungal mycelium growth is likely to exhibit some variability in the architecture and distribution of the mycelium formed, even under the same specimen preparation and growth conditions. As such the values of hydraulic properties presented here are not intended to be used for design but are a first step towards understanding the types of soil modification that can be induced by fungal treatment of granular materials. Indeed, it is recommended that future studies investigate the variability of hydraulic performance of fungal treated specimens under replicate conditions and in varying nutrient and environmental conditions.

The X-μCT imaging conducted in this study has provided valuable insight into the pore modifications that can be induced by fungal mycelium growth. However, future studies will seek to explore phase-contrast tomography or heavy metal staining, emerging techniques for the study of 3D biological structures (Rawson et al., 2020), in order to improve the attenuation contrast between fungal mycelium and nutrient (carbon) substrates.

5.4 Potential for in-situ applications

Our results indicate the potential for fungal mycelium growth to be engineered in soils for the purpose of reducing infiltration in granular soils. Such a technology could have application in the treatment of hillslopes where failures are triggered in response to wetting in order to maintain higher soil suction and higher shear strength at depth following rainfall events. Indeed, the low dry density of the soil mixture used in this study (1080kg/m^3) was motivated by the low dry densities which can be found in the near surface soil layers of natural hillslopes.

For example, Balzano et al., (2019) reported dry densities in the range of 300-750kg/m^3 in the top 1m of soil (including cohesionless soil layers) for a hillslope susceptible to recurrent landslides. Fungal treatment at catchment-scale would be relatively low-cost and could be carried out in a manner similar to hydro-seeding, spraying fungal spores/hyphal suspension alongside a carbon nutrient source.

P. ostreatus can grow extensively and increases in biomass within available pore space as long as environmental conditions are suitable (Salifu, 2019). In this study, *P. ostreatus* was inoculated into soil with an adequate carbon supply and water content and incubated at 25°C based on optimal growth conditions determined in Salifu (2019). After 12 weeks growth period, fungal induced water repellency still persists in the soil (Salifu and El Mountassir, 2020) and there was evidence of massive hyphal colonisation of soils (Figure 9b). Evidence of continued fungal activity was observed in forms of fresh whitish patches of mycelial growth during the 48-day period of the drying-wetting cycles and the X-μCT images indicate that even 16 months after inoculation, with no further supply of nutrients, the mycelium remains extensive, as seen in Figure 11. These observations of continuous/prolonged mycelial activity observed in the treated specimen lends support to the argument that a soil improvement strategy based on fungal mycelium would require minimal intervention, provided that suitable environmental conditions exist.

6 Conclusion

This study was undertaken to determine the influence of the growth of *P. ostreatus* on the soil-water retention behaviour, ponded infiltration behaviour and quasi-saturated hydraulic conductivity of a sand amended with organic matter (lignocellulose), 12 weeks after fungal inoculation. An untreated control was set-up and compared with the treated specimen to determine the extent of modification to the soil hydraulic properties due to fungal growth. Findings from this work are:

1. Fungal treatment resulted in modifications to the soil water retention behaviour, such that wetting curves were shifted to lower suctions and drying curves shifted to higher suctions due to combined biochemical and biophysical effects of fungal growth.

2. Fungal treated soil resulted in significantly lower infiltration rates compared to that obtained in untreated soil. This is attributed to clogging of some of the pore network by hyphal biomass and the hydrophobic biochemical secretions which act to increase the advancing contact angle in part of the pore network. These combined characteristics resulted in, significant delay in advancement of the wetting front, lower overall infiltration rate and the formation of preferential flow through tortuous paths in the treated sand.
3. Due to the very low initial dry density (1.08g cm^{-3}) of these specimens, the untreated specimen exhibited a volumetric collapse of 10% upon infiltration as it transitioned towards a saturated state and soil suction was reduced. In contrast the treated specimen exhibited only 1% volumetric collapse. The presence of hyphae and their enmeshment of the sand particles had a stabilising effect on the arrangement of soil particles during infiltration.
4. The quasi-saturated hydraulic conductivity (k_s) for the fungal treated soil was found to be an order of magnitude lower than the k_s for the untreated soil.

The results presented in this paper illustrate the potential for the deployment of fungal treated soils as a low cost, low carbon technique for reducing infiltration into slopes, or for creating semi-permeable layers deployable in the design of slow draining water holding layers in capillary barriers or as surface layers in geo-infrastructures utilised for water diversion purposes.

Acknowledgement

The authors wish to acknowledge the support of the European Commission via the Marie Skłodowska-Curie Innovative Training Networks (ITN-ETN) project TERRE 'Training Engineers and Researchers to Rethink geotechnical Engineering for a low carbon future' (H2020-MSCA-ITN-2015-675762); and the Engineering and Physical Sciences Research Council via Grant EP/N035526/1.

Data Statement

Data associated with this publication are openly available from the University of Strathclyde KnowledgeBase at https://doi.org/xxxxxxxxxxxx/.

References

Angers, D. A. and Caron, J. (1998). 'Plant-induced changes in soil structure: Processes and feedbacks', *Biogeoechemistry,* 42:55-72.

Antinori, M. E. *et al.* (2020) 'Fine-Tuning of Physicochemical Properties and Growth Dynamics of Mycelium-Based Materials', *ACS Applied Bio Materials*, 3(2), pp. 1044–1051. doi: 10.1021/acsabm.9b01031.

Arganda-Carreras, I. *et al.* (2017) 'Trainable Weka Segmentation: a machine learning tool for microscopy pixel classification', *Bioinformatics*, 33(15), pp. 2424–2426. doi: 10.1093/bioinformatics/btx180.

Balzano, B., Tarantino, A. and Ridley, A. (2019) 'Preliminary analysis on the impacts of the rhizosphere on occurrence of rainfall-induced shallow landslides', *Landslides*, 16(10), pp. 1885–1901. doi: 10.1007/s10346-019-01197-5.

Barden, L., McGown, A. and Collins, K. (1973) 'The collapse mechanism in partly saturated soil', *Engineering Geology*, 7(1), pp. 49–60. doi: 10.1016/0013-7952(73)90006-9.

Bauters, T. W. J. *et al.* (2000) 'Physics of water repellent soils', *Journal of Hydrology*, 231–232, pp. 233–243. doi: 10.1016/S0022-1694(00)00197-9.

Beckett, C., Fourie, A. and Toll, D. (2016) 'Water repellent soils: The case for unsaturated soil mechanics', *E3S Web of Conferences*, 9. doi: 10.1051/e3sconf/20160911011.

Boldrin, D., Leung, A. K. and Bengough, A. G. (2020) 'Hydro-mechanical reinforcement of contrasting woody species: a full-scale investigation of a field slope', *Géotechnique*, pp. 1–15. doi: 10.1680/jgeot.19.sip.018.

BS EN ISO 14688-2:2018. Geotechnical investigation and testing. Identification and classification of soil. Principles for a classification. (2018).

Crawford, J. W. *et al.* (2012) 'Microbial diversity affects self-organization of the soil - Microbe system with consequences for function', *Journal of the Royal Society Interface*, 9(71), pp. 1302–1310. doi: 10.1098/rsif.2011.0679.

Fourie, A. B., Rowe, D. and Blight, G. E. (1999) 'The effect of infiltration on the stability of the slopes of a dry ash dump', *Geotechnique*, 49(1), pp. 1–13. doi: 10.1680/geot.1999.49.1.1.

Ghestem, M., Sidle, R. C. and Stokes, A. (2011) 'The Influence of Plant Root Systems on Subsurface Flow: Implications for Slope Stability', *BioScience*, 61(11), pp. 869–879. doi: 10.1525/bio.2011.61.11.6.

Greenwood, J. R., Norris, J. E. and Wint, J. (2004) 'Assessing the contribution of vegetation to slope stability', *Proceedings of the Institution of Civil Engineers - Geotechnical Engineering*, 157(4), pp. 199–207. doi: 10.1680/geng.2004.157.4.199.

Hughes, P. N. *et al.* (2009) 'Full-scale testing to assess climate effects on embankments', in *Proceedings of the Institution of Civil Engineers: Bridge Engineering*, pp. 67–79. doi: 10.1680/ensu.2009.162.2.67.

Islam, M. R. *et al.* (2018) 'Publisher Correction: Morphology and mechanics of fungal mycelium', *Scientific Reports*, 8(1). doi: 10.1038/s41598-018-20637-1.

Kallio, J. M., Linder, M. B. and Rouvinen, J. (2007) 'Crystal structures of hydrophobin HFBII in the presence of detergent implicate the formation of fibrils and monolayer films', *Journal of Biological Chemistry*, 282(39), pp. 28733–28739. doi: 10.1074/jbc.M704238200.

Keatts, M. I. *et al.* (2018) 'Apparent contact angle and water entry head measurements for organo-silane modified sand and coal fly ash', *Journal of Geotechnical and Geoenvironmental Engineering*, 144(6). doi: 10.1061/(ASCE)GT.1943-5606.00.

Leung, A.K., Gard, A., Coo, J. L., Ng, C.W.W. and Hau, B.C.H. (2015). 'Effects of the roots of *Cynodon dactylon* and *Schefflera heptaphylla* on water infiltration and soil hdyraulic conductivity', *Hydrol. Process.* 29, 3342-3354. doi: 10.1002/hyp.10452.

Linder, M. B. *et al.* (2005) 'Hydrophobins: The protein-amphiphiles of filamentous fungi', *FEMS Microbiology Reviews*, 29(5), pp. 877–896. doi: 10.1016/j.femsre.2005.01.004.

Lourenço, S. D. N., Wang, G. H. and Kamai, T. (2015) 'Processes in model slopes made of mixtures of wettable and water repellent sand: Implications for the initiation of debris flows in dry slopes', *Engineering Geology*. Elsevier B.V., 196, pp. 47–58. doi: 10.1016/j.enggeo.2015.06.021.

Lu, J., Zhang, Q., Werner, A. D., Li, Y., Jiang, S. and Tan, Z. (2020) 'Root-induced changes of soil hydraulic properties - A Review' *J. Hydrol.* 589: 125203. https://doi.org/10.1016/j.jhydrol.2020.125203

Mardhiah, U. *et al.* (2016) 'Arbuscular mycorrhizal fungal hyphae reduce soil erosion by surface water flow in a greenhouse experiment', *Applied Soil Ecology*, 99, pp. 137–140. doi: 10.1016/j.apsoil.2015.11.027.

Minagawa, H. *et al.* (2008) 'Characterization of sand sediment by pore size distribution and permeability using proton nuclear magnetic resonance measurement', *Journal of Geophysical Research: Solid Earth*, 113(7). doi: 10.1029/2007JB005403.

Ng, C. W. W. *et al.* (2013) 'Experimental investigation of induced suction distribution in a grass-covered soil', *Ecological Engineering*, 52, pp. 219–223. doi: 10.1016/j.ecoleng.2012.11.013.

Nimmo, J. R. *et al.* (2009) 'Rapid Measurement of Field-Saturated Hydraulic Conductivity for Areal Characterization', *Vadose Zone Journal*, 8(1), pp. 142–149. doi: 10.2136/vzj2007.0159.

Olivares, L. and Picarelli, L. (2004) 'Shallow flowslides triggered by intense rainfalls on natural slopes covered by loose unsaturated pyroclastic soils', *Géotechnique*, 53(2), pp. 283–287. doi: 10.1680/geot.53.2.283.37268.

Orozco, L. F. and Caicedo, B. (2017) 'Water migration in unsaturated partially hydrophobic soils', *Géotechnique Letters*, 7(1), pp. 18–23. doi: 10.1680/jgele.16.00105.

Pagano, A. G., Tarantino, A. and Magnanimo, V. (2018a) 'A microscale-based model for small-strain stiffness in unsaturated granular geomaterials', *Géotechnique*, pp. 1–54. doi: 10.1680/jgeot.17.p.238.

Pagano, A. G., Tarantino, A. and Magnanimo, V. (2018b) 'A microscale-based model for small-strain stiffness in unsaturated granular geomaterials', *Géotechnique*, pp. 1–14. doi: 10.1680/jgeot.17.p.238.

Pajor, R. (2012) 'Quantification of short term interactions between soil and fungi .', (March).

Pollen-Bankhead, N. and Simon, A. (2010) 'Hydrologic and hydraulic effects of riparian root networks on streambank stability: Is mechanical root-reinforcement the whole story?', *Geomorphology*, 116(3–4), pp. 353–362. doi: 10.1016/j.geomorph.2009.11.013.

Rawson, S.D., Maksimcuka, J., Withers, P.J. *et al.* X-ray computed tomography in life sciences. *BMC Biol* **18,** 21 (2020). https://doi.org/10.1186/s12915-020-0753-2

Rillig, M. C. and Mummey, D. L. (2006) 'Tansley review Mycorrhizas and soil structure', pp. 41–53. doi: 10.1111/j.1469-8137.2006.01750.x.

Salifu, E. (2019) *Engineering Fungal-Mycelia for Soil Improvement*. PhD Thesis, University of Strathclyde, Glasgow, United Kingdom.

Salifu, E. and El Mountassir, G. (2020) 'Fungal-induced water repellency in sand', *Géotechnique*, Accepted(In press), pp. 1–8. doi: 10.1680/jgeot.19.p.341.

Schindelin, J. *et al.* (2015) 'The ImageJ ecosystem: An open platform for biomedical image analysis', *Molecular Reproduction and Development*, 82(7–8), pp. 518–529. doi: 10.1002/mrd.22489.

Scotto di Santolo, A., Evangelista, L. and Evangelista, A. (2017) 'Gravity retaining walls in unsaturated pyroclastic materials: Observations and numerical modeling', *Rivista Italiana di Geotecnica*, 51(1), pp. 26–42.

Shokri, N., Lehmann, P. and Or, D. (2009) 'Characteristics of evaporation from partially wettable porous media', *Water Resources Research*, 45(2), pp. 1–12. doi: 10.1029/2008WR007185.

Springman, S. M., Jommi, C. and Teysseire, P. (2004) 'Instabilities on moraine slopes induced by loss of suction: a case history', *Géotechnique*, 53(1), pp. 3–10. doi: 10.1680/geot.53.1.3.37260.

Stanier, S. A. and Tarantino, A. (2013) 'An approach for predicting the stability of vertical cuts in cohesionless soils above the water table', *Engineering Geology*, 158, pp. 98–108. doi: 10.1016/j.enggeo.2013.03.012.

Stokes, A. *et al.* (2013) 'Engineering the ecological mitigation of hillslope stability research into the scientific literature', *Ecological Engineering*, 61, pp. 615–620. doi: 10.1016/j.ecoleng.2013.07.065.

Talbot, N. J., Ebbole, D. J. and Hamer, J. E. (1993) 'Identification and characterization of MPG1, a gene involved in pathogenicity from the rice blast fungus Magnaporthe grisea', *Plant Cell*, 5(11), pp. 1575–1590. doi: 10.1105/tpc.5.11.1575.

Tisdall, J. M. *et al.* (2012) 'Stabilisation of soil against wind erosion by six saprotrophic fungi', *Soil Biology and Biochemistry*. Elsevier Ltd, 50, pp. 134–141. doi: 10.1016/j.soilbio.2012.02.035.

Veylon, G. *et al.* (2015) 'Quantification of mechanical and hydric components of soil reinforcement by plant roots', *Canadian Geotechnical Journal*. NRC Research Press, 52(11), pp. 1839–1849. doi: 10.1139/cgj-2014-0090.

Vogelsang, K. M. *et al.* (2004) *The Use of Mycorrhizal Fungi in Erosion Control Applications*, *Contract Report*. Available at: https://pdfs.semanticscholar.org/3c44/156d03c80e327913c06fac4fa8084d5584d0.pdf?_ga=2.216907669.2012585161.1572648647-240717194.1572648647.

Waldron, L. J. (1977) 'The Shear Resistance of Root-Permeated Homogeneous and Stratified Soil', *Soil Science Society of America Journal*, 41(5), pp. 843–849. doi: 10.2136/sssaj1977.03615995004100050005x.

Wang, Z. *et al.* (2003) 'Effects of water repellency on infiltration rate and flow instability', *Soil Water Repellency: Occurrence, Consequences, and Amelioration*, 232, pp. 235–244. doi: 10.1016/B978-0-444-51269-7.50024-2.

Wang, Z., Wu, L. and Wu, Q. J. (2000) 'Water-entry value as an alternative indicator', *Journal of Hydrology*, pp. 76–83. doi: 10.1016/B978-0-444-51269-7.50009-6.

Wessels, J. G. H. *et al.* (1991) 'The thn mutation of Schizophyllum commune, which suppresses formation of aerial hyphae, affects expression of the Sc3 hydrophobin gene', *Journal of General Microbiology*, 137(10), pp. 2439–2445. doi: 10.1099/00221287-137-10-2439.

Wessels, J. G. H. (1996) 'Hydrophobins: Proteins that Change the Nature of the Fungal Surface', in *Advances in microbial physiology*. Academic Press, pp. 1–45. doi: 10.1016/s0065-2911(08)60154-x.

Wessels, J. G. H. (2000) 'Hydrophobins, unique fungal proteins', *Mycologist*, 14(4), pp. 153–159.

Wösten, H. A. B. (2001) 'Hydrophobins: Multipurpose Proteins', *Annual Review of Microbiology*, 55(1), pp. 625–646. doi: 10.1146/annurev.micro.55.1.625.

Zheng, S. *et al.* (2017) 'Hydrologic behavior of model slopes with synthetic water repellent soils', *Journal of Hydrology*. Elsevier B.V., 554, pp. 582–599. doi: 10.1016/j.jhydrol.2017.09.013.

881 Zheng, S. *et al.* (2019) 'Erodibility of synthetic water repellent granular materials: Adapting
882 the ground to weather extremes', *Science of the Total Environment*, 689, pp. 398–412. doi:
883 10.1016/j.scitotenv.2019.06.328.

884